Spatial and temporal distribution characteristics and ozone formation potentials of volatile organic compounds from three typical functional areas in China

Hao Luo, Guiying Li, Jiangyao Chen, Qinhao Lin, Shengtao Ma, Yujie Wang, Taicheng An*

Guangdong Key Laboratory of Environmental Catalysis and Health Risk Control, Guangzhou Key Laboratory of Environmental Catalysis and Pollution Control, School of Environmental Science and Engineering, Institute of Environmental Health and Pollution Control, Guangdong University of Technology, Guangzhou, 510006, China

ABSTRACT

Background: Ozone is currently one of the most important air pollutants. Volatile organic compounds (VOCs) can easily react with atmospheric radicals to form ozone. In-field measurement of VOCs may help in estimating the local VOC photochemical pollution level.

Method: This study examined the spatial and temporal distribution characteristics of VOCs during winter at three typical sites of varying classification in China; industrial (Guangzhou Economic and Technological Development District (GETDD)), urban (Guangzhou higher education mega center (HEMC)), and rural (Pingyuan county (PYC)), using Proton-Transfer-Reaction Time-of-Flight Mass Spectrometry (PTR-ToF-MS).

Results: The concentrations of total VOCs (TVOCs) at the GETDD, HEMC and PYC sites were 352.5, 129.2 and 75.1 ppb, respectively. The dominant category of VOCs is nitrogen-containing VOCs (NVOCs, accounting for 43.3% of TVOCs) at GETDD, of which $C_4H_{11}N$ (m/z^+ = 74.10, butyl amine) was the predominant chemical species (80.5%). In contrast, oxygenated VOCs (OVOCs) were the most abundant at HEMC and PYC, accounting for 60.2% and 64.1% of the total VOCs, respectively; here, CH_4O (m/z^+ = 33.026, methanol) was the major compound, accounting for 40.5% of the VOCs at HEMC and 50.9% at PYC. The ratios of toluene to benzene (T/B) were calculated for different measured sites, as the ratios of T/B can reveal source resolution of aromatic VOCs. The average contributions to total ozone formation potentials (OFP) of the total measured VOCs in each area were 604.9, 315.9 and 111.7 $\mu g/m^3$ at GETDD, HEMC and PYC, respectively; the highest OFP contributors of the identified VOCs were aliphatic hydrocarbons (AlHs) at GETDD, aromatic hydrocarbons (AHs) at HEMC, and OVOCs at PYC.

Conclusions: OFP assessment indicated that the photochemical pollution caused by VOCs at GETDD was serious, and was also significant in the HEMC region. The dominant VOC OFP groups (AlHs and AHs) should be prioritized for control, in order to help reduce these effects.

1. Introduction

With increased development of cities and industrialization in China, atmospheric pollution in urban air is becoming an ever more increasing issue. Volatile organic compounds (VOCs) are an important group of atmospheric pollutants, and undergo complex photochemical processes with NO_x or free radicals in the troposphere (Malecha and Nizkorodov, 2016; Zhu et al., 2017). In particular, VOCs are essential precursors of photochemical reactions which produce ozone, peroxyaceylnitrate (PAN), and other oxides and secondary organic aerosols (Atkinson and Arey, 2003). Furthermore, plenty of studies on the relationships between VOCs and near-ground-ozone have been recently performed,

revealing that the formation of ozone is sensitive to precursor atmospheric VOCs (Guo et al., 2017; Wu et al., 2016; Zhao et al., 2018), and VOCs are regarded as critical ozone precursors as defined by the United States Environmental Protection Agency (USEPA) (Shao et al., 2016). In addition, the toxicities of several VOCs (benzene, toluene, and 1,3-butadiene) have been documented; these compounds exhibit harmful effects on human health, including nose, throat, and lung irritation, asthma, and can even lead to death (Knox, 2005; Li et al., 2017). Because of these concerns, it is urgently important to understand the spatial and temporal distribution characteristics of VOCs in the ambient atmosphere (Gao et al., 2018).

Generally, offline sampling methods are widely used in atmospheric

---

VOC field observations (An et al., 2014; Chen et al., 2016c, 2019; Liu et al., 2019a). Gas chromatography/mass spectrometry (GC/MS) with preconcentration steps can effectively detect and measure VOC constituents in the atmosphere (Chen et al., 2016b; He et al., 2012; Liu et al., 2017, Liu et al., 2019b). However, some problems have arisen with using these offline processing methods, including the loss of sample during transit due to volatility as well as low time resolution (Han et al., 2019; Zhu et al., 2019). Comparatively, proton transfer reaction time-of-flight mass spectrometry (PTR-ToF-MS) has recently been developed for the easy, real-time detection of atmospheric VOCs (Hansela et al., 1995; Lindinger et al., 1998). The description of this method as well as applications to online quantitative detection of VOCs have been detailed in previous reviews (Blake et al., 2009; de Gouw and Warneke, 2007). Moreover, PTR-ToF-MS is more suitable for the online detection of VOCs due to the various advantages it provides, including higher resolution and avoiding sample pretreatment. Furthermore, this technology is also superior for determining some of the more uncommon VOCs that lack reference standards, such as oxygenated VOCs (OVOCs) and nitrogen-containing VOCs (NVOCs) (Han et al., 2019). OVOCs in particular are important ozone precursors that cannot be effectively measured using traditional methods (An et al., 2014).

The primary objective of this study was to investigate the pollution profile of atmospheric VOCs and their ozone formation potentials (OFP) during the diurnal variations at different functional areas in China. To understand the characteristic pollutants at three selected sampling sites, PTR-ToF-MS was used for continuous real-time VOC online monitoring. The component distribution and concentrations of VOCs were obtained at the three sampling sites, and the ratio of toluene to benzene (T/B) was used to study the source resolution and the photochemical aging processes of the air mass at some of the functional areas with high levels of these two compounds. Furthermore, the chemical reactivity of VOCs was also comparatively evaluated by calculating the corresponding OFP at these three functional areas.

2. Material and methods

2.1. Sampling sites and descriptions

To investigate the spatial distribution differences of VOCs between urban and rural areas, three sites around China were selected based on their unique primary activities. Guangzhou is a typical crowded metropolis in Southern China, where both natural and anthropogenic emission sources of VOCs existed. Two sites in Guangzhou, including Guangzhou Economic and Technological Development District (GETDD) and Guangzhou higher education mega center (HEMC), were selected. GETDD is located in the industrial zone, and its air quality is likely to be primarily influenced by industrial emission, whereas HEMC is an area defined by higher education institutions with substantial afforested areas, but less industrial activity. In contrast, Pingyuan county (PYC) in Shandong province is a representative rural area in the plain of Northern China, where one of the most significant emission sources of VOCs is likely the open burning of agricultural-waste (biomass burning). Despite the differences in winter meteorological conditions between Guangzhou and Shandong, we chose the most representative rural area of the North China plain as the rural point source to illustrate the differences between agricultural sources and urban sources, and background and industrial sources. The detailed information of these three areas is given in Fig. S1 and Table S1.

2.2. Sampling and analytical methodology

At each of the three sites, VOC sampling and measurement was conducted using PTR-ToF-MS 1000 (Ionicon Analytik GmbH Innsbruck, Austria) under continuous operation. Samples were collected continuously on each day from November 9, 2017 to January 9, 2018 at PYC, from January 16 to January 22, 2018 at HEMC, and from February

3 to February 9, 2018 at GETDD.

Ambient air samples were directly drawn through a 2 m long polyetheretherketone (PEEK) tube placed outside with a constant temperature of 20–25 °C. Sampled air was inhaled into the reaction drift tube of the PTR-ToF-MS via a 1.5 m long PEEK tube heated at 80 °C with a flow rate of approximately 30 mL/min. The key operating parameters were as follows: 2.3 mbar pressure, 80 °C, and 600 V in the drift tube. A corresponding E/N ratio of approximately 130 Td (E = electric field strength, N = gas number density, 1 Td = 10^{-17} V cm^2) was obtained with these parameters. Protonated water (H_3O^+) was used as the reagent ion for the proton-transfer reaction. In this mode, VOCs with a proton affinity higher than that of water were measured, including aromatic hydrocarbons, acids, and carbonyls. Detailed information about PTR-ToF-MS can be found in previous works (Graus et al., 2010; Klein et al., 2018). The mass spectra up to 240 m/z was recorded with TOF-DAQ software (Tofwerk AG, Switzerland), and the signal intensities (cps) of raw data were converted into ppb concentrations for each VOC using the formula described previously (Lindinger et al., 1998) in TOF-DAQ (Tofwerk AG, Switzerland). Before sampling, the calibration of the PTR-ToF-MS was conducted according to the standard sample PAMs and TO-15 (Linde Spectra Environment Gases, USA), and the background value of the instrument was measured by introducing high purity nitrogen (99.999%). The detection limits were specified to be less than 0.01 ppb according to the instrument manual. The instrument was calibrated every week, and instrument preparation methodology has been detailed in our previous studies (Han et al., 2019).

2.3. Ozone formation potential

As a product of VOCs and free radical reactions, ozone is closely related to VOCs (Kumar et al., 2018; Tan et al., 2018). Different VOC species significantly vary in their potential to form ozone, and OFP is normally used to describe the contribution of VOCs to ozone generation (Liu et al., 2019a; Ou et al., 2015; Wu and Xie, 2017). Here, the OFP of VOCs was calculated using "maximum incremental reactivity" (MIR) coefficients as follows (Carter, 2008, 2010):

$$OFP_i = Con(VOC_i) \times MIR_i \qquad (1)$$

where OFP_i is defined as the OFP of VOC_i (μg/m^3), MIR_i is the maximum incremental reactivity coefficient of the VOC_i (gm ozone/gm VOCs) which was obtained from previous references (Carter, 2008, 2010), and $Con(VOC_i)$ is the concentration of VOC_i (μg/m^3).

3. Results and discussion

3.1. Long-term observation of VOCs level at three different functional areas

To understand the VOC pollution profiles, the VOCs observed in the three different functional areas were grouped into different classes; aromatic hydrocarbons (AHs), aliphatic hydrocarbons (AlHs), NVOCs and OVOCs (including 58 kinds of VOCs with standards, as well as other identified and quantified VOCs by PTR-ToF-MS). Fig. 1 shows the concentrations of total VOCs (TVOCs) and relative contributions of main groups of VOCs at the three different sampling sites. The concentrations were the average concentration of different groups of VOCs observed over the total sampling period.

The air was heavily polluted at the GETDD site, with a TVOC concentration of 352.5 ppb. Comparatively, the pollution at the HEMC and PYC sites was much lower, with TVOC concentrations of 129.2 and 75.1 ppb, respectively. Specifically, at the GETDD site, NVOCs (152.6 ppb) and OVOCs (130.5 ppb) were the two predominant groups, accounting for 43.3% and 37.0% of TVOCs, respectively; comparatively, AHs and AlHs were not as high. At the HEMC and PYC sites, OVOCs were the most important contributors to TVOCs, and were
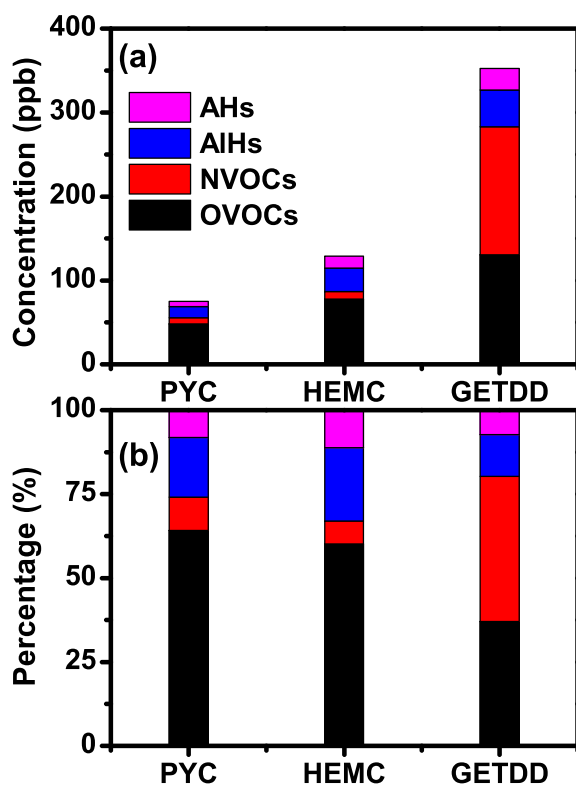
Fig. 1. Concentrations (a) and relative contributions (b) of VOC species sampling at PYC, HEMC and GETDD as measure with PTR-ToF-MS during sampling processes.

found in proportions of 60.2% and 64.1%, respectively. Unlike at the GETDD site, NVOCs at the HEMC and PYC sites were minor, while AlHs were second highest component of the TVOC content (21.8% and 17.7%, respectively). The high proportion of OVOCs and AlHs at the PYC and HEMC sites could be mainly caused by release from grass and vegetation (Bao et al., 2008; Yu et al., 2008). In addition, it is worth mentioning that as the proton affinity of alkanes below C3, and alkenes below C2, is weaker than that of water, PTR-ToF-MS cannot obtain measurements of these four hydrocarbons (methane, ethane, propane and ethylene); as such, the obtained levels of AlHs might be underestimated in the current study. However, in general, the concentrations of different VOC species at the GETDD site were much higher than that at the HEMC and PYC sites.

Further analysis was also carried out to determine the pollution profile of individual VOCs of different categories (Figs. S2–S5). Among NVOCs (Fig. S2) at the GETDD site, the most abundant component was $C_4H_{11}N$ ($m/z^+ = 74.10$, butyl amine), accounting for 80.5% of the total NVOC concentration. The second-most predominant NVOC was hydrogen cyanide (HCN, $m/z^+ = 28.018$), accounting for 9.0%, and the remaining 10 + species made up only 10.5% of the total NVOCs. It has been reported that organic amines are mainly released from anthropogenic sources, such as solvent evaporation in factories (Mao et al., 2018; Yao et al., 2016). Organic amines have been proven to play a significant role in new particle formation and growth from various chamber experiments, theoretical calculations, and field observations (Chen et al., 2016a; Jen et al., 2016; You et al., 2014). In contrast, at the HEMC and PYC sites, HCN was the main contributor and accounted for 45.9% and 78.3% of total NVOC concentration, respectively. Previous studies found that HCN is an important component in gasoline vehicle emissions in the HEMC area (Baum et al., 2007; Moussa et al., 2016). As such, we can conclude that some gasoline vehicle emissions exist at the HEMC and PYC sites, although the level of NVOCs is very low in these areas. In addition, a small portion of C_2H_3N ($m/z^+ = 42.034$,

acetonitrile) was also identified at both the HEMC (8.3%) and PYC (5.3%) sites, which may be from biological emissions and biomass burning (Hui et al., 2018; Li et al., 2018; Wood et al., 2010).

Among OVOCs (Fig. S3), C_3H_6O ($m/z^+ = 59.049$, acetone) was the most abundant, accounting for 56.9% at the GETDD site; this is probably due to solvent evaporation during industrial processes in the area. However, at the HEMC and PYC sites, the most abundant OVOC was CH_4O ($m/z^+ = 33.026$, methanol), accounting for 40.5% and 50.9% of total OVOC concentration, respectively. This proportion can be attributed to the significant anthropogenic primary sources in these areas, such as household solvents and biomass combustion (Zhu et al., 2019).

As for the AlHs category (Fig. S4), C_4H_6 ($m/z^+ = 55.0542$) accounted for the highest proportion (56.1% of total AlHs) at the GETDD site, which may be due to industrial emissions (Jia et al., 2016; Zhu et al., 2018); a high proportion (30.2%) of C_3H_6 ($m/z^+ = 43.054$) was also detected at this site. In contrast, at the HEMC and PYC sites, C_3H_6 was the predominant species, accounting for 49.2% and 38.9% of total AlHs, respectively. C_3H_6 can result from both natural and anthropogenic sources, such as volatile organic solvents and industrial process at GETDD, fossil fuels and biological processes at HEMC, and combustion processes at PYC. It is worth noting that C_5H_8 ($m/z^+ = 69.07$, isoprene) accounted for 5.0% of AlHs at HEMC, which was higher than at the other two sites sampled; this likely indicates that biological emissions and photochemical reactions at HEMC site are more significant contributors (Kaltsonoudis et al., 2016; Sahu and Saxena, 2015).

Among AHs (Fig. S5), the collective group of C_6H_6 ($m/z^+ = 79.054$, benzene), C_7H_8 ($m/z^+ = 93.070$, toluene), C_8H_{10} ($m/z^+ = 107.048$, C8-aromatics), and C_9H_{12} ($m/z^+ = 121.10$, C9-aromatics) accounted for 92.5% (HEMC), 96.5% (GETDD), and 89.1% (PYC) of the total of AHs. Toluene in particular was the most abundant AH component identified at GETDD, which may come from anthropogenic sources such as vehicle exhaust and solvent evaporation in industrial production processes.

In this study, we also employed a simple identification method to judge VOC sources through the diagnostic ratios of benzene, toluene, ethylbenzene, and xylenes (BTEX) (Ma et al., 2016; Zheng et al., 2018; Zhu et al., 2019). BTEX are mainly emitted from industrial activities, vehicle exhausts, and chemical solvents (Dumanoglu et al., 2014). As it is impossible to distinguish the isomers of C_8H_{10} (ethylbenzene and o/m/p-xylene) using PTR-ToF-MS, the correlation with BTEX was calculated according to the concentrations of C_6H_6 (benzene), C_7H_8 (toluene), and C_8H_{10} (ethylbenzene and o/m/p-xylene). As Table S2 shows, excellent correlation between benzene and ethylbenzene/xylene ($R^2 = 0.8555$) was found at the GETDD site, but poor correlation was seen between toluene and benzene ($R^2 = 0.1480$) and between toluene and ethylbenzene/xylene ($R^2 = 0.2056$) was found. These results indicate that some complicated sources exist for BTEX that appeared at different times, or only emitted at a certain time at the GETDD site. Toluene, in particular, is an essential substance in the production process in factories at the GETDD site; therefore, mixed emission sources of BTEX can reasonably explain the poor correlations between toluene and benzene/ethylbenzene/xylene at the GETDD site. Comparatively, good correlations were found among BTEX compounds ($R^2 > 0.8877$) at the HEMC site, indicating that VOCs here were mainly caused by vehicle exhausts, as benzene mainly results from traffic emissions while toluene and ethylbenzene/xylene mainly result from traffic sources and industrial solvents (Marc et al., 2016; Yuan et al., 2010; Zhang et al., 2013). Without nearby point sources, this urban background site might be affected by anthropogenic pollution, which is likely dominated by vehicle exhausts. At the PYC site, the correlations ($0.6876 > R^2 > 0.6250$) among BTEX indicated that vehicle exhaust was not the main source of these compounds in the region. Overall, good correlations among BTEX compounds were obtained at all investigated sites except at the GETDD site, where weak correlations between benzene and toluene as well as between benzene and ethylbenzene/xylene were
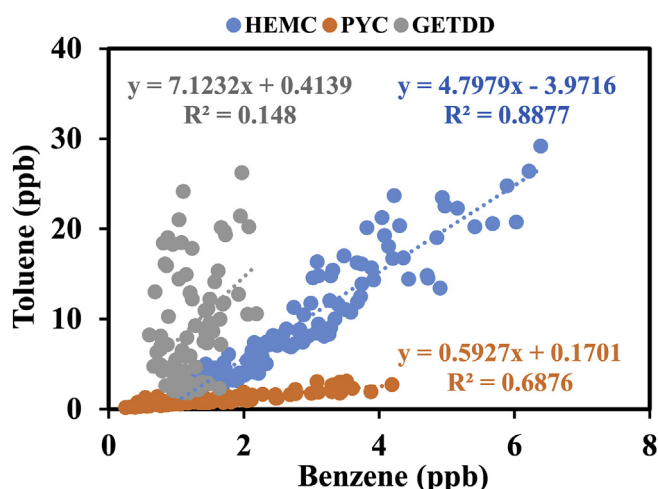
Fig. 2. The correlation between toluene and benzene in the PYC, HEMC and GETDD.

identified, indicating that sources of VOCs varied at the GETDD site, but were consistent at the HEMC and PYC sites.

As vehicle emissions were found to be the main cause of AHs in this study, which is in accordance with previous findings (Wang et al., 2016), benzene was selected as an indicator for AHs. Correlations between toluene and benzene were found to be better at the HEMC and PYC sites than at the GETDD site (Fig. 2), indicating that mixed sources of toluene, such as the evaporation of solvents, along with traffic emissions existed at this site. A higher slope was obtained at the GETDD site than at the HEMC and PYC sites, which may further indicate that other important point sources exist at this site besides motor vehicle exhaust (Kumar et al., 2018).

In the air, toluene and benzene can be attenuated by reaction with $^{\bullet}OH$; the reaction rate of toluene with $^{\bullet}OH$ is five times higher than that of benzene (Atkinson, 2000; Atkinson and Arey, 2003). Because of this, the ratio of toluene to benzene (T/B ratio) can be used to study the source resolution as well as the photochemical aging process of localized air masses (Hui et al., 2018; Niu et al., 2012). Generally, T/B ≤ 2 indicates that VOCs are mainly caused by automotive exhaust emissions, while T/B > 2 indicates that other sources also contribute (Jia et al., 2016; Suthawaree et al., 2012). Here, T/B ratios were found to be 7.46, 3.41, and 0.75 at the GETDD, HEMC, and PYC sites, respectively, indicating that the GETDD site was significantly impacted by local and/or regional source emissions (Zhang et al., 2013); this mirrored our observations that higher amounts of toluene were discharged from the factories surrounding this site.

The time-resolved individual VOCs profiles were also examined for each site, and formaldehyde, acetonitrile and isoprene were selected as tracer VOCs (Hui et al., 2018; Mo et al., 2017; Sarkar et al., 2016). Figs. 3, S6, and S7 show the temporal trends of individual VOCs, with the hourly average concentrations of eight VOCs (C_5H_8, C_3H_6O, C_2H_3N, CH_2O, C_6H_6, C_7H_8, C_8H_{10}, and C_9H_{12}). At GETDD site, C_3H_6O, C_2H_3N, and CH_2O generally had similar trends (Fig. 3). Concentrations were relatively high on February 5, 2018 between 19:00–21:00, then decreased sharply on February 6, 2018 between 0:00–2:00 before reaching another high on February 6, 2018 between 6:00–7:00. In addition, aromatics (including C_6H_6, C_8H_{10}, and C_9H_{12}) had two relatively high periods on February 6, 2018 between 0:00–7:00 and from February 6, 2018 at 21:00 to February 7, 2018 at 2:00. Toluene concentrations were high during the entire sampling period at the GETDD site, and aromatic compounds, i.e. toluene (9.78 and 9.21 ppb, respectively) was the most abundant species at GETDD and HEMC, followed next by ethylbenzene (3.11 and 8.19 ppb, respectively). The results seen here are similar to those measured in Hebei (Sun et al., 2018) and reflect the complex characteristics of local emissions at
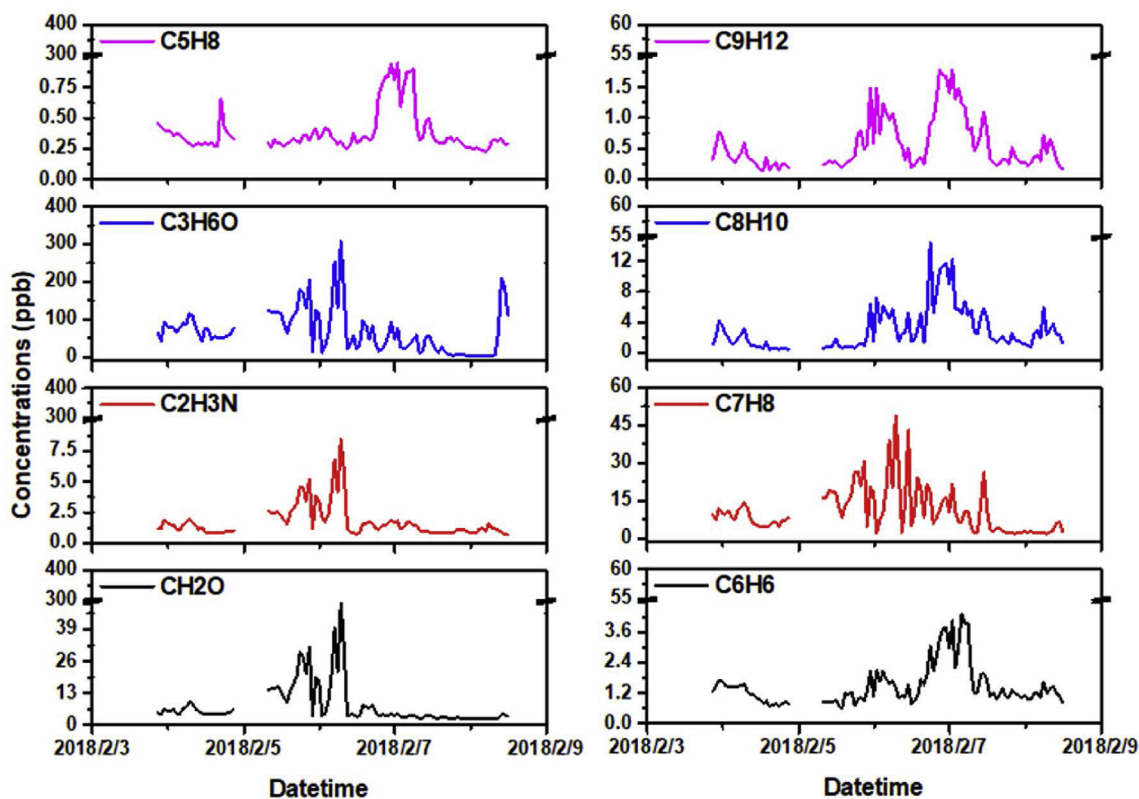

Fig. 3. The time series variation of selected VOCs at GETDD: represented time series of formaldehyde (CH_2O), acetonitrile (C_2H_3N), acetone (C_3H_6O), isoprene (C_5H_8) and.
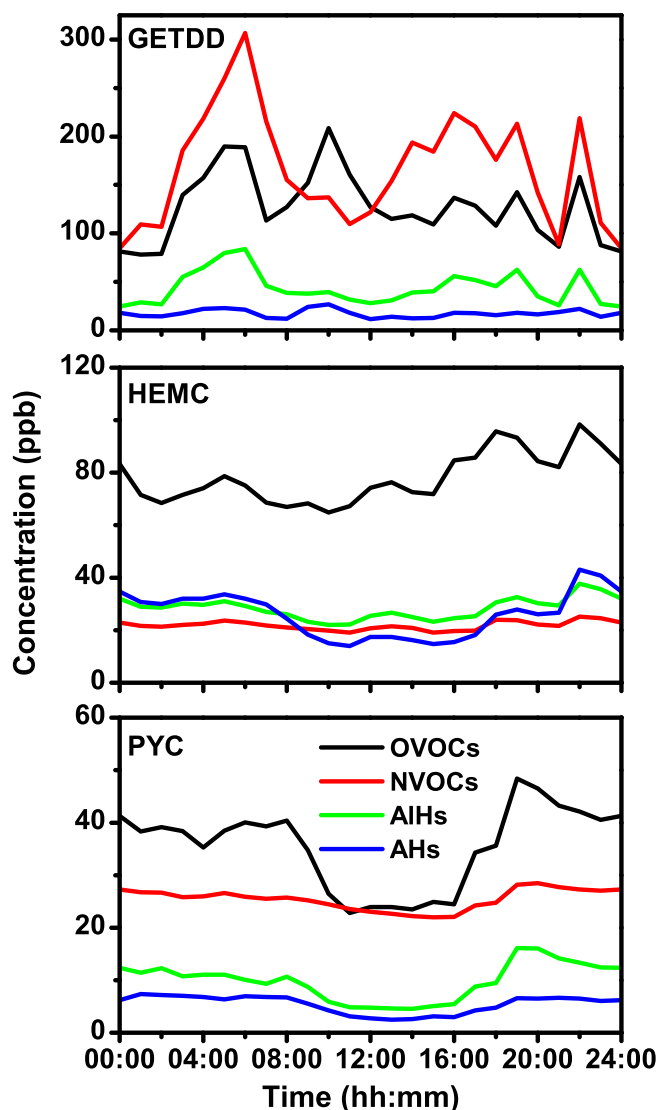
Fig. 4. The average diurnal variation of the total concentration of the four categories VOCs (AHs, AlHs, NVOCs and OVOCs) at PYC, HEMC and GETDD.

sampling sites, as benzene and toluene are major components of both exhaust and common solvents (Barletta et al., 2002; Jobson et al., 2004).

At both the PYC and HEMC sites, C_5H_8, C_3H_6O, C_2H_3N, and CH_2O had similar trends within each site (Figs. S8 and S9). A relatively high level of VOCs was found at PYC site between December 6–7 and December 9–10, 2017. Concentrations dropped to their lowest on December 10, 2017, before another spike in concentration was observed between December 27–31, 2017. Similar temporal trends in aromatics (including C_6H_6, C_7H_8, C_8H_{10}, and C_9H_{12}) were also found at PYC site within the same period; the concentrations of toluene (C_7H_8) and ethylbenzene (C_8H_{10}) between December 28–29, 2017 were much higher than the mean values (1.45 and 1.95 ppb, respectively). Besides the accidental emissions due to pollution dispersion, the increase of C_7H_8 and C_8H_{10} concentrations seen during the daytime may also have been caused by anthropogenic emissions such as vehicle discharge near the sampling sites. At HEMC site, benzene, toluene, C8-aromatics, and C9-aromatics showed similar trends to C_5H_8, C_3H_6O, C_2H_3N, and CH_2O during the full sampling period (Fig. S6). The highest concentrations were reached at 6:00–8:00 before dropping rapidly on 11:00–13:00, January 18, 2018. A similar phenomenon was also seen on January 19 and 22, 2018, though not on the Saturday and Sunday between. We

believe that the increase of VOCs at HEMC during this time was mainly due to anthropogenic sources during the workday, which is why the "weekend effects" were observed (Hui et al., 2018). The concentration variation of VOCs at the three sites was closely related to local production and living activities, and the corresponding characteristics that differ between sites are likely associated with these factors; as a city site, HEMC is obviously affected by vehicle exhaust, while GETDD is affected by motor vehicle exhaust as well as regional industrial production.

3.2. Diurnal variation of VOCs

To further study the pollution characteristics of the studied VOCs, the average per-hour diurnal variations of total concentrations for the four VOC categories (AHs, AlHs, NVOCs, and OVOCs) at three sites calculated (Fig. 4). The concentration of each group fluctuated widely, with different trends observed between 00:00 to 24:00. NVOCs and OVOCs at GETDD site were much higher than at the other two studied sites; here NVOCs were highest during most of the studied period, followed by OVOCs, AlHs, and AHs, respectively. The concentrations of NVOCs and AlHs were up to the highest at 7:00, while OVOCs and AHs were highest at 10:00; this may be due to the influence of the factory working hours at this site, as well as the increase of vehicle exhaust emissions during 9:00–10:00. Comparatively, at HEMC site, the concentration of OVOCs was approximately two times higher than that of AHs, AlHs, and NVOCs, which underwent much lower fluctuations. It is worth noting that the concentration of AHs was higher at 7:00, and increased from approximately 17:00, potentially due to vehicle exhaust during rush hour at this site. At PYC site, two spikes in concentrations of the OVOCs, AlHs, and AHs were observed from 6:00 to 8:00 and from 18:00 to 21:00, which may be attributed to the biomass burning nearby. Here, AlHs, NVOCs, and OVOCs increased to their highest respective concentrations at 4:00–6:00 (see Fig. 5).

The complex composition and concentrations of VOCs, as well as the chemical reaction activities of the different components, could potentially lead to different diurnal variations. Therefore, the diurnal variation curves of typical individual VOC in four categories were also displayed (Figs. 5, S8, and S9). Compared with PYC and HEMC sites, the diurnal variations of isoprene and toluene at the GETDD site were much lower, while the concentration of formaldehyde and acetonitrile peaked at 5:00 before increasing again to another peak at 19:30. Between 12:00–14:00, the concentrations of the four tracer VOCs all dropped to their respective minimums, potentially due to oxidation between VOCs and ·OH (Tang et al., 2007). In this study, it is worth mentioning that the concentrations of almost all VOC components were higher during daytime than at night, which is consistent with previous results (Xu et al., 2017). This may be because photochemical processes play a substantial role in VOC transformation, and because of the dilution effect of boundary layer development.

Comparatively, at HEMC site, the average diurnal distribution of typical VOCs shows obvious variations (Fig. S9). Formaldehyde concentrations remained steady before sunrise, increased from approximately 07:00–08:00, and peaked in the afternoon (approximately 12:00–15:00), before then gradually returning to a stable value at night. This trend is similar to results in Shenzhen city, and is highly related to the formation of secondary pollution from atmospheric oxidation (Wang et al., 2017). Similar to the PYC site (Fig. S8), the diurnal distribution of acetonitrile and toluene at HEMC site gradually decreased with the enhancement of solar light intensity at 11:00–14:00, and then rose from 16:00 to reach peak values at 23:00. The concentration of isoprene at HEMC site was higher than at the other two sites, with insignificant diurnal variation.

The average diurnal variations of each species fluctuated widely at the PYC site, which is an average representative rural area in Northern China (Fig. S8). Each VOC had a similar trend in variation, and the fluctuation period was highly consistent with the biomass combustion
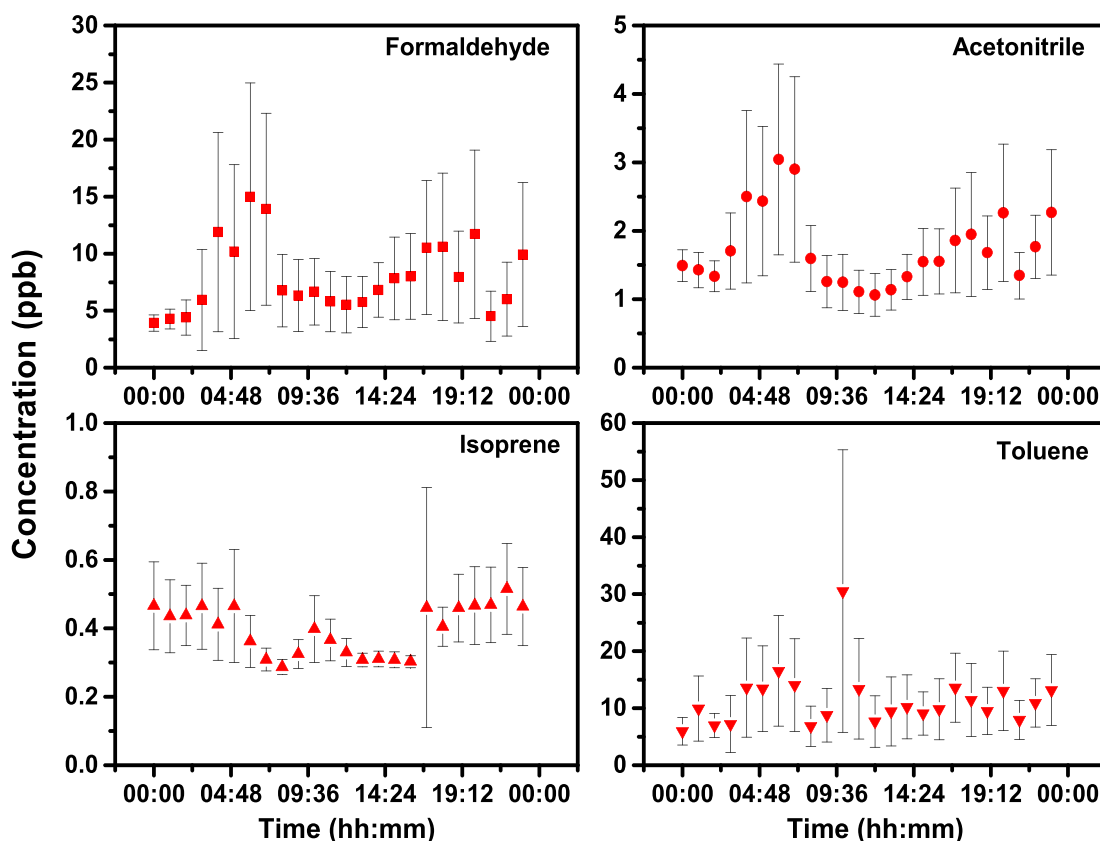
Fig. 5. The average diurnal variation of VOCs at GETDD: represented species of formaldehyde (CH_2O), acetonitrile (C_2H_3N), isoprene (C_5H_8) and toluene (C_7H_8).
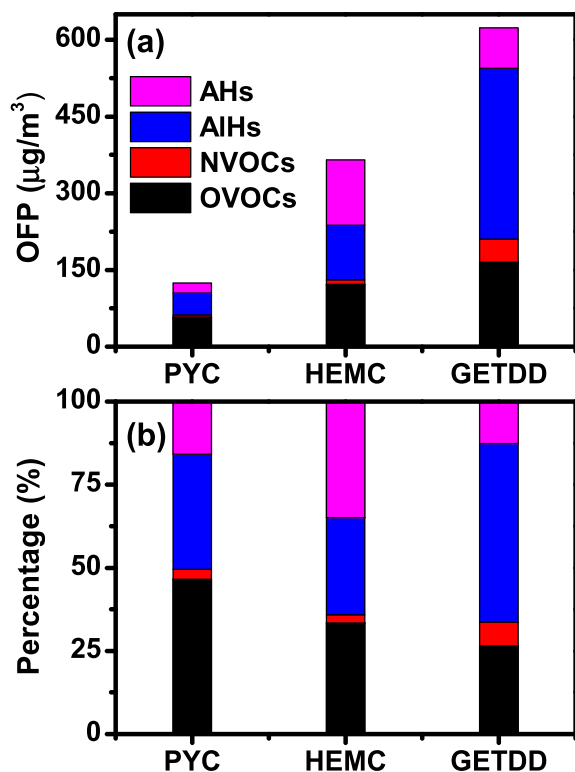

Fig. 6. The (a) total ozone formation potentials and (b) their proportion of the four categories VOCs (AHs, AlHs, NVOCs and OVOCs) at PYC, HEMC and GETDD.

period in the region. Furthermore, lower concentrations of VOCs were observed during the day, likely resulting from the photochemical oxidation of VOC by ˙OH (Tang et al., 2007). Acetonitrile in particular is widely regarded as a VOC marker for biomass combustion (Sarkar et al., 2016). The average hourly concentration of acetonitrile appeared to peak at 7: 00 and 18:00 at the PYC site, indicating these periods were likely peak times for biomass combustion. The concentration of toluene rebounded at night; this is likely due to the weakening of photochemical reactions during this period because of lower ˙OH and vehicular emissions during the night (Lyu et al., 2016). The diurnal variation of formaldehyde was similar to that of the other tracer VOCs, likely because this compound is generated by photochemical oxidation processes from the direct-discharge and reactive VOCs.

3.3. Ozone formation potentials

Total OFPs were calculated for the sites according to the average concentrations of different groups of VOCs over the observation period (Fig. 6). As expected, the total OFP at GETDD was much higher than that seen at the other two sites; overall, the total OFPs ranged from 336.9 to 1165.3 $\mu g/m^3$ (average: 604.9 $\mu g/m^3$), 229.7–440.7 $\mu g/m^3$ (average: 315.9 $\mu g/m^3$), and 64.7–159.8 $\mu g/m^3$ (average: 111.7 $\mu g/m^3$) at GETDD, HEMC and PYC sites, respectively. The OFP results indicated that the photochemical pollution caused by VOCs at GETDD was serious, and that, while not as significant as that seen at GETDD, this problem also existed at HEMC.

At GETDD site, the main contributors to the OFP were AlHs (53.6%) and OVOCs (26.6%). These were different from the VOC pollution profile for this site, where NVOCs and OVOCs were the two predominant groups (Fig. 1). Similar phenomena were also observed at the other two sites, where the pollution profile did not correlate with the main contributors to the OFP; this indicated that the contribution of NVOCs to the OFP was very minor, while the other three groups (in
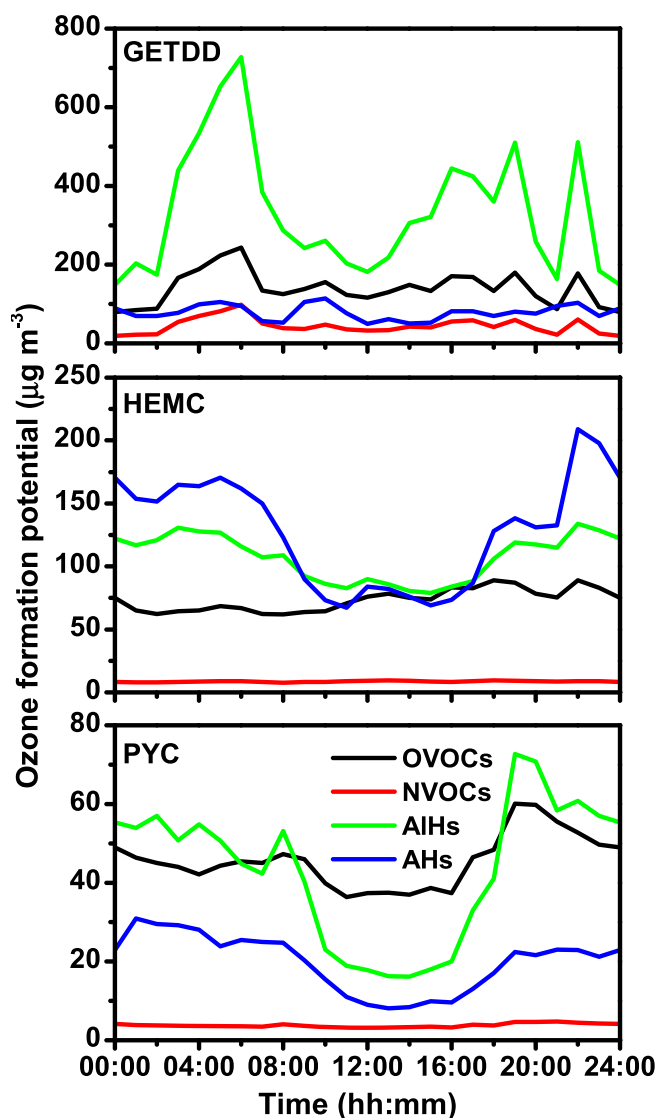
Fig. 7. The average diurnal variation of the ozone formation potentials of the four categories VOCs (AHs, AlHs, NVOCs and OVOCs) at PYC, HEMC and GETDD.

particular AlHs) played very important roles. This is because the MIRs of the AlHs were much higher than for the other VOC species; as such, the contribution of AlHs to the OFP was much higher, even though their concentrations were not the most abundant. These findings are consistent with previous knowledge, as AHs have typically been found to be the most important VOC species in terms of OFP contribution in urban areas (such as HEMC), while AlHs are the primary contributors in industrial areas (such as GETDD) (Tan et al., 2018).

Specifically, butadiene (accounting for 48.1% of total OFP), C8-aromatics (17.4%) and formaldehyde (21.1%) were the dominant VOCs contributing to ozone formation at GETDDD, HEMC, and PYC sites, respectively. In addition, the OFP of butadiene (290.8 $\mu g/m^3$) at GETDD site was significantly higher than at both at PYC (14.1 $\mu g/m^3$) and HEMC (32.4 $\mu g/m^3$) sites. Butadiene is known to be related to industrial production, and therefore, it is expected that it would have been emitted from factories at this site, since GETDD is one of the top three industrial production bases within the chemical industry in China (Mo et al., 2015). In addition, although the MIR values of C9-aromatics and isoprene were very high, their contribution to the ozone levels at all three sampling sites was less than 4% due to their low ambient concentrations. In contrast, low OFP values were obtained for other VOCs

(such as methanol, acetone and benzene) because of their low MIR values, although their ambient concentrations were very high.

To further understand the variation in OFP as it related to the time of day, the diurnal variations in OFP for four VOC categories at GETDD, HEMC and PYC sites were also analyzed. The highest level of OFP appeared around 6:00 at the GETDD site (Fig. 7), which may have been caused by vehicle exhaust emissions and industrial discharge at this time (including solvent evaporation). Comparatively, at HEMC site, higher values of OFP appeared between 4:00–8:00, but then decreased to their lowest levels around 10:00–16:00 before finally increasing from 16:00 to reach their peak value at 22:00. These fluctuations indicate that at this site, vehicle exhaust emissions during rush hour (6:00–8:00 and 16:00–18:00) as well as biological emissions at night likely were responsible for the patterns observed. At the PYC site, the period of high OFP levels was much shorter (around 6:00–8:00), following which the OFP decreased gradually after 8:00 until it reached its lowest point at 14:00 (though a second peak did appear at 19:00). The main reason for this may be that the variation of OFP levels during the daytime at this site in particular was mainly caused by biomass burning, which occurs during these times. In conclusion, the AlHs and OVOCs at the GETDD site, the AHs at the HEMC site, and the OVOCs and AlHs at the PYC site deserve the attention of the local environmental protection agencies in order to better control pollution in these areas according to their primary functional activities. The formation of relevant VOC control policies should fundamentally consider the causes of local daily variations in VOC in a given area in order for these policies to most effectively address the problems particular to that region.

4. Conclusion

The concentrations of ambient VOCs at three sites in China were analyzed using PTR-ToF-MS during the winter period from November 9, 2017 to February 9, 2018. TVOCs were found in the highest concentration at the GETDD > HEMC > PYC sites. The NVOCs were found as the highest proportion of VOCs measured at the GETDD site, followed by the OVOCs. Comparatively, OVOCs accounted for the highest proportion of TVOCs at both the PYC and HEMC sites. The evaluation of OFP revealed that the photochemical pollution caused by VOCs at GETDD was serious, and was also significant at HEMC. AlHs were the VOC species with the highest OFP in the industrial area (GETDD), while AHs were more important contributors in urban areas (HEMC). These dominant OFP-contributing VOC groups (AlHs and AHs) should therefore be given priority in terms of controlling their emission. In the future, online monitoring of VOCs in the industrial zone will need to be carried out in real time to better understand pollution, and targeted control policies should be enforced effectively depending on the primarily contributing VOCs in a respective area.

Appendix A. Supplementary data

Supplementary data to this article can be found online at https://doi.org/10.1016/j.envres.2020.109141.

References

An, T., Huang, Y., Li, G., He, Z., Chen, J., Zhang, C., 2014. Pollution profiles and health risk assessment of VOCs emitted during e-waste dismantling processes associated with different dismantling methods. Environ. Int. 73, 186–194.

Atkinson, R., 2000. Atmospheric chemistry of VOCs and NOx. Atmos. Environ. 34, 2063–2101.

Atkinson, R., Arey, J., 2003. Gas-phase tropospheric chemistry of biogenic volatile organic compounds: a review. Atmos. Environ. 37, 197–219.

Bao, H., Kondo, A., Kaga, A., Tada, M., Sakaguti, K., Inoue, Y., Shimoda, Y., Narumi, D., Machimura, T., 2008. Biogenic volatile organic compound emission potential of forests and paddy fields in the Kinki region of Japan. Environ. Res. 106, 156–169.

Barletta, B., Meinardi, S., Simpson, I.J., Khwaja, H.A., Blake, D.R., Rowland, F.S., 2002. Mixing ratios of volatile organic compounds (VOCs) in the atmosphere of Karachi, Pakistan. Atmos. Environ. 36, 3429–3443.

Baum, M.M., Moss, J.A., Pastel, S.H., Poskrebyshev, G.A., 2007. Hydrogen cyanide exhaust emissions from in use motor vehicles. Environ. Sci. Technol. 41, 857–862.

Blake, R.S., Monks, P.S., Ellis, A.M., 2009. Proton-transfer reaction mass spectrometry. Chem. Rev. 109, 861–896.

Carter, W.P.L., 2008. Reactivity Estimates for Selected Consumer Product Compounds. The California Air Resources Board Contracts.

Carter, W.P.L., 2010. Development of the SAPRC-07 Chemical Mechanism and Updated Ozone Reactivity Scales. The California Air Resources Board Contracts.

Chen, H., Ma, S., Yu, Y., Liu, R., Li, G., Huang, H., An, T., 2019. Seasonal profiles of atmospheric PAHs in an e-waste dismantling area and their associated health risk considering bioaccessible PAHs in the human lung. Sci. Total Environ. 683, 371–379.

Chen, H., Varner, M.E., Gerber, R.B., Finlayson-Pitts, B.J., 2016a. Reactions of methanesulfonic acid with amines and ammonia as a source of new particles in air. J. Phys. Chem. B 120, 1526–1536.

Chen, J., Huang, Y., Li, G., An, T., Hu, Y., Li, Y., 2016b. VOCs elimination and health risk reduction in e-waste dismantling workshop using integrated techniques of electrostatic precipitation with advanced oxidation technologies. J. Hazard Mater. 302, 395–403.

Chen, J., Zhang, D., Li, G., An, T., Fu, J., 2016c. The health risk attenuation by simultaneous elimination of atmospheric VOCs and POPs from an e-waste dismantling workshop by an integrated de-dusting with decontamination technique. Chem. Eng. J. 301, 299–305.

de Gouw, J., Warneke, C., 2007. Measurements of volatile organic compounds in the earth's atmosphere using proton-transfer-reaction mass spectrometry. Mass Spectrom. Rev. 26, 223–257.

Dumanoglu, Y., Kara, M., Altiok, H., Odabasi, M., Elbir, T., Bayram, A., 2014. Spatial and seasonal variation and source apportionment of volatile organic compounds (VOCs) in a heavily industrialized area. Atmos. Environ. 98, 168–178.

Gao, J., Zhang, J., Li, H., Li, L., Xu, L., Zhang, Y., Wang, Z., Wang, X., Zhang, W., Chen, Y., Cheng, X., Zhang, H., Peng, L., Chai, F., Wei, Y., 2018. Comparative study of volatile organic compounds in ambient air using observed mixing ratios and initial mixing ratios taking chemical loss into account - a case study in a typical urban area in Beijing. Sci. Total Environ. 628–629, 791–804.

Graus, M., Muller, M., Hansel, A., 2010. High resolution PTR-TOF: quantification and formula confirmation of VOC in real time. J. Am. Soc. Mass Spectrom. 21, 1037–1044.

Guo, H., Ling, Z.H., Cheng, H.R., Simpson, I.J., Lyu, X.P., Wang, X.M., Shao, M., Lu, H.X., Ayoko, G., Zhang, Y.L., Saunders, S.M., Lam, S.H.M., Wang, J.L., Blake, D.R., 2017. Tropospheric volatile organic compounds in China. Sci. Total Environ. 574, 1021–1043.

Han, C., Liu, R., Luo, H., Li, G., Ma, S., Chen, J., An, T., 2019. Pollution profiles of volatile organic compounds from different urban functional areas in Guangzhou China based on GC/MS and PTR-TOF-MS: atmospheric environmental implications. Atmos. Environ. 116843.

Hansela, A., Jordana, A., Holzingera, R., Prazellera, P., Vogelb, W., Lindingera, W., 1995. Proton transfer reaction mass spectrometry: on-line trace gas analysis at the ppb level. Int. J. Mass Spectrom. Ion Process. 149–150, 609–619.

He, Z., Li, J., Chen, J., Chen, Z., Li, G., Sun, G., An, T., 2012. Treatment of organic waste gas in a paint plant by combined technique of biotrickling filtration with photocatalytic oxidation. Chem. Eng. J. 200–202, 645–653.

Hui, L., Liu, X., Tan, Q., Feng, M., An, J., Qu, Y., Zhang, Y., Jiang, M., 2018. Characteristics, source apportionment and contribution of VOCs to ozone formation in Wuhan, Central China. Atmos. Environ. 192, 55–71.

Jen, C.N., Bachman, R., Zhao, J., McMurry, P.H., Hanson, D.R., 2016. Diamine-sulfuric acid reactions are a potent source of new particle formation. Geophys. Res. Lett. 43, 867–873.

Jia, C., Mao, X., Huang, T., Liang, X., Wang, Y., Shen, Y., Jiang, W., Wang, H., Bai, Z., Ma, M., Yu, Z., Ma, J., Gao, H., 2016. Non-methane hydrocarbons (NMHCs) and their contribution to ozone formation potential in a petrochemical industrialized city, Northwest China. Atmos. Res. 169, 225–236.

Jobson, B.T., Berkowitz, C.M., Kuster, W.C., Goldan, P.D., Williams, E.J., Fesenfeld, F.C., Apel, E.C., Karl, T., Lonneman, W.A., Riemer, D., 2004. Hydrocarbon source signatures in Houston, Texas: influence of the petrochemical industry. J. Geophys. Res. 109. https://doi.org/10.1029/2004JD004887.

Kaltsonoudis, C., Kostenidou, E., Florou, K., Psichoudaki, M., Pandis, S.N., 2016. Temporal variability and sources of VOCs in urban areas of the eastern Mediterranean. Atmos. Chem. Phys. 16, 14825–14842.

Klein, F., Pieber, S.M., Ni, H., Stefenelli, G., Bertrand, A., Kilic, D., Pospisilova, V., Temime-Roussel, B., Marchand, N., El Haddad, I., Slowik, J.G., Baltensperger, U., Cao, J., Huang, R.J., Prevot, A.S.H., 2018. Characterization of gas-phase organics using proton transfer reaction time-of-flight mass spectrometry: residential coal combustion. Environ. Sci. Technol. 52, 2612–2617.

Knox, E.G., 2005. Childhood cancers and atmospheric carcinogens. J. Epidemiol. Community Health 59, 101–105.

Kumar, A., Singh, D., Kumar, K., Singh, B., Bihari, Jain, Kumar, V., 2018. Distribution of VOCs in urban and rural atmospheres of subtropical India_ Temporal variation, source attribution, ratios, OFP and risk assessment. Sci. Total Environ. 613–614 492-451.

Li, B., Ho, S.S.H., Xue, Y., Huang, Y., Wang, L., Cheng, Y., Dai, W., Zhong, H., Cao, J., Lee, S., 2017. Characterizations of volatile organic compounds (VOCs) from vehicular emissions at roadside environment: the first comprehensive study in Northwestern China. Atmos. Environ. 161, 1–12.

Li, J., Zhai, C., Yu, J., Liu, R., Li, Y., Zeng, L., Xie, S., 2018. Spatiotemporal variations of ambient volatile organic compounds and their sources in Chongqing, a mountainous megacity in China. Sci. Total Environ. 627, 1442–1452.

Lindinger, W., Hansel, A., Jordan, A., 1998. Proton-transfer-reaction mass spectrometry (PTR–MS): on-line monitoring of volatile organic compounds at pptv levels. Chem. Soc. Rev. 27, 347–354.

Liu, R., Chen, J., Li, G., An, T., 2017. Using an integrated decontamination technique to remove VOCs and attenuate health risks from an e-waste dismantling workshop. Chem. Eng. J. 318, 57–63.

Liu, R., Chen, J., Li, G., Wang, X., An, T., 2019a. Cutting down on the ozone and SOA formation as well as health risks of VOCs emitted from e-waste dismantlement by integration technique. J. Environ. Manag. 249, 107755.

Liu, R., Ma, S., Li, G., Yu, Y., An, T., 2019b. Comparing pollution patterns and human exposure to atmospheric PBDEs and PCBs emitted from different e-waste dismantling processes. J. Hazard Mater. 369, 142–149.

Lyu, X.P., Chen, N., Guo, H., Zhang, W.H., Wang, N., Wang, Y., Liu, M., 2016. Ambient volatile organic compounds and their effect on ozone production in Wuhan, central China. Sci. Total Environ. 541, 200–209.

Ma, Y., Diao, Y., Zhang, B., Wang, W., Ren, X., Yang, D., Wang, M., Shi, X., Zheng, J., 2016. Detection of formaldehyde emissions from an industrial zone in the Yangtze-River-Delta region of China using a proton transfer reaction ion-drift chemical ionization mass spectrometer. Atmos. Meas. Tech. Discuss. https://doi.org/10.5194/amt-9-6101-2016.

Malecha, K.T., Nizkorodov, S.A., 2016. Photodegradation of secondary organic aerosol particles as a source of small, oxygenated volatile organic compounds. Environ. Sci. Technol. 50, 9990–9997.

Mao, J., Yu, F., Zhang, Y., An, J., Wang, L., Zheng, J., Yao, L., Luo, G., Ma, W., Yu, Q., Huang, C., Li, L., Chen, L., 2018. High-resolution modeling of gaseous methylamines over a polluted region in China: source-dependent emissions and implications of spatial variations. Atmos. Chem. Phys. 18, 7933–7950.

Marc, M., Bielawska, M., Simeonov, V., Namiesnik, J., Zabiegala, B., 2016. The effect of anthropogenic activity on BTEX, NO₂, SO₂, and CO concentrations in urban air of the spa city of Sopot and medium-industrialized city of Tczew located in North Poland. Environ. Res. 147, 513–524.

Mo, Z., Shao, M., Lu, S., Niu, H., Zhou, M., Sun, J., 2017. Characterization of non-methane hydrocarbons and their sources in an industrialized coastal city, Yangtze River Delta, China. Sci. Total Environ. 593–594, 641–653.

Mo, Z., Shao, M., Lu, S., Qu, H., Zhou, M., Sun, J., Gou, B., 2015. Process-specific emission characteristics of volatile organic compounds (VOCs) from petrochemical facilities in the Yangtze River Delta, China. Sci. Total Environ. 533, 422–431.

Moussa, S.G., Leithead, A., Li, S.M., Chan, T.W., Wentzell, J.J.B., Stroud, C., Zhang, J., Lee, P., Lu, G., Brook, J.R., Hayden, K., Narayan, J., Liggio, J., 2016. Emissions of hydrogen cyanide from on-road gasoline and diesel vehicles. Atmos. Environ. 131, 185–195.

Niu, Z., Zhang, H., Xu, Y., Liao, X., Xu, L., Chen, J., 2012. Pollution characteristics of volatile organic compounds in the atmosphere of haicang District in xiamen city, southeast China. J. Environ. Monit. 14, 1145–1152.

Ou, J., Zheng, J., Li, R., Huang, X., Zhong, Z., Zhong, L., Lin, H., 2015. Speciated OVOC and VOC emission inventories and their implications for reactivity-based ozone control strategy in the Pearl River Delta region, China. Sci. Total Environ. 530–531, 393–402.

Sahu, L.K., Saxena, P., 2015. High time and mass resolved PTR-TOF-MS measurements of VOCs at an urban site of India during winter: role of anthropogenic, biomass burning, biogenic and photochemical sources. Atmos. Res. 164–165, 84–94.

Sarkar, C., Sinha, V., Kumar, V., Rupakheti, M., Panday, A., Mahata, K.S., Rupakheti, D., Kathayat, B., Lawrence, M.G., 2016. Overview of VOC emissions and chemistry from PTR-TOF-MS measurements during the SusKat-ABC campaign: high acetaldehyde, isoprene and isocyanic acid in wintertime air of the Kathmandu Valley. Atmos. Chem. Phys. 16, 3979–4003.

Shao, P., An, J., Xin, J., Wu, F., Wang, J., Ji, D., Wang, Y., 2016. Source apportionment of VOCs and the contribution to photochemical ozone formation during summer in the typical industrial area in the Yangtze River Delta, China. Atmos. Res. 176–177, 64–74.

Sun, J., Wang, Y., Wu, F., Tang, G., Wang, L., Wang, Y., Yang, Y., 2018. Vertical characteristics of VOCs in the lower troposphere over the North China Plain during pollution periods. Environ. Pollut. 236, 907–915.

Suthawaree, J., Tajima, Y., Khunchornyakong, A., Kato, S., Sharp, A., Kajii, Y., 2012. Identification of volatile organic compounds in suburban Bangkok, Thailand and their potential for ozone formation. Atmos. Res. 104–105, 245–254.

Tan, Z., Lu, K., Jiang, M., Su, R., Dong, H., Zeng, L., Xie, S., Tan, Q., Zhang, Y., 2018. Exploring ozone pollution in Chengdu, southwestern China: a case study from radical chemistry to O₃-VOC-NOx sensitivity. Sci. Total Environ. 636, 775–786.

Tang, J.H., Chan, L.Y., Chan, C.Y., Li, Y.S., Chang, C.C., Liu, S.C., Wu, D., Li, Y.D., 2007. Characteristics and diurnal variations of NMHCs at urban, suburban, and rural sites in

the Pearl River Delta and a remote site in South China. Atmos. Environ. 41, 8620–8632.

Wang, C., Huang, X.F., Han, Y., Zhu, B., He, L.Y., 2017. Sources and potential photochemical roles of formaldehyde in an urban atmosphere in South China. J. Geophys. Res.: Atmos. 122, 11934–911947.

Wang, G., Cheng, S., Wei, W., Zhou, Y., Yao, S., Zhang, H., 2016. Characteristics and source apportionment of VOCs in the suburban area of Beijing, China. Atmos. Pollut. Res. 7, 711–724.

Wood, E.C., Canagaratna, M.R., Herndon, S.C., Onasch, T.B., Kolb, C.E., Worsnop, D.R., Kroll, J.H., Knighton, W.B., Seila, R., Zavala, M., Molina, L.T., DeCarlo, P.F., Jimenez, J.L., Weinheimer, A.J., Knapp, D.J., Jobson, B.T., Stutz, J., Kuster, W.C., Williams, E.J., 2010. Investigation of the correlation between odd oxygen and secondary organic aerosol in Mexico City and Houston. Atmos. Chem. Phys. 10, 8947–8968.

Wu, F., Yu, Y., Sun, J., Zhang, J., Wang, J., Tang, G., Wang, Y., 2016. Characteristics, source apportionment and reactivity of ambient volatile organic compounds at Dinghu Mountain in Guangdong Province, China. Sci. Total Environ. 548–549, 347–359.

Wu, R., Xie, S., 2017. Spatial distribution of ozone formation in China derived from emissions of speciated volatile organic compounds. Environ. Sci. Technol. 51, 2574–2583.

Xu, Z., Huang, X., Nie, W., Chi, X., Xu, Z., Zheng, L., Sun, P., Ding, A., 2017. Influence of synoptic condition and holiday effects on VOCs and ozone production in the Yangtze River Delta region, China. Atmos. Environ. 168, 112–124.

Yao, L., Wang, M.Y., Wang, X.K., Liu, Y.J., Chen, H.F., Zheng, J., Nie, W., Ding, A.J., Geng, F.H., Wang, D.F., Chen, J.M., Worsnop, D.R., Wang, L., 2016. Detection of atmospheric gaseous amines and amides by a high-resolution time-of-flight chemical ionization mass spectrometer with protonated ethanol reagent ions. Atmos. Chem. Phys. 16, 14527–14543.

You, Y., Kanawade, V.P., de Gouw, J.A., Guenther, A.B., Madronich, S., Sierra-Hernández, M.R., Lawler, M., Smith, J.N., Takahama, S., Ruggeri, G., Koss, A., Olson, K.,

Baumann, K., Weber, R.J., Nenes, A., Guo, H., Edgerton, E.S., Porcelli, L., Brune, W.H., Goldstein, A.H., Lee, S.H., 2014. Atmospheric amines and ammonia measured with a chemical ionization mass spectrometer (CIMS). Atmos. Chem. Phys. 14, 12181–12194.

Yu, Y., Wen, S., Lu, H., Feng, Y., Wang, X., Sheng, G., Fu, J., 2008. Characteristics of atmospheric carbonyls and VOCs in forest park in South China. Environ. Monit. Assess. 137, 275–285.

Yuan, B., Shao, M., Lu, S., Wang, B., 2010. Source profiles of volatile organic compounds associated with solvent use in Beijing, China. Atmos. Environ. 44, 1919–1926.

Zhang, Y., Wang, X., Barletta, B., Simpson, I.J., Blake, D.R., Fu, X., Zhang, Z., He, Q., Liu, T., Zhao, X., Ding, X., 2013. Source attributions of hazardous aromatic hydrocarbons in urban, suburban and rural areas of the Pearl River Delta (PRD) region. J. Hazard Mater. 250–251, 403–411.

Zhao, X., Cheng, H., He, S., Cui, X., Pu, X., Lu, L., 2018. Spatial associations between social groups and ozone air pollution exposure in the Beijing urban area. Environ. Res. 164, 173–183.

Zheng, H., Kong, S., Xing, X., Mao, Y., Hu, T., Ding, Y., Li, G., Liu, D., Li, S., Qi, S., 2018. Monitoring of volatile organic compounds (VOCs) from an oil and gas station in northwest China for 1 year. Atmos. Chem. Phys. 18, 4567–4595.

Zhu, B., Han, Y., Wang, C., Huang, X., Xia, S., Niu, Y., Yin, Z., He, L., 2019. Understanding primary and secondary sources of ambient oxygenated volatile organic compounds in Shenzhen utilizing photochemical age-based parameterization method. J. Environ. Sci. 75, 105–114.

Zhu, H., Wang, H., Jing, S., Wang, Y., Cheng, T., Tao, S., Lou, S., Qiao, L., Li, L., Chen, J., 2018. Characteristics and sources of atmospheric volatile organic compounds (VOCs) along the mid-lower Yangtze River in China. Atmos. Environ. 190, 232–240.

Zhu, Y., Yang, L., Kawamura, K., Chen, J., Ono, K., Wang, X., Xue, L., Wang, W., 2017. Contributions and source identification of biogenic and anthropogenic hydrocarbons to secondary organic aerosols at Mt. Tai in 2014. Environ. Pollut. 220, 863–872.